

Fast acquisition of left and right ventricular function parameters applying cardiovascular magnetic resonance in clinical routine – validation of a 2-shot compressed sensing cine sequence

Jan Gröschel^{a,b} , Clemens Ammann^{a,b} , Leonora Zange^{a,c}, Darian Viezzer^{a,b}, Christoph Forman^d, Michaela Schmidt^d, Edyta Blaszczyk^{a,b} and Jeanette Schulz-Menger^{a,b,c}

^aCharité – Universitätsmedizin Berlin, Corporate Member of Freie Universität Berlin, Humboldt-Universität zu Berlin, and Berlin Institute of Health, Working Group on Cardiovascular Magnetic Resonance, Experimental and Clinical Research Center, a Joint Cooperation Between the Charité Medical Faculty and the Max-Delbrück Center for Molecular Medicine Charité Campus Buch, Berlin, Germany; ^bDZHK (German Centre for Cardiovascular Research), Partner Site Berlin, Berlin, Germany; ^cDepartment of Cardiology and Nephrology, HELIOS Hospital Berlin-Buch, Berlin, Germany; ^dSiemens Healthineers, Erlangen, Germany

ABSTRACT

Objectives. To evaluate if cine sequences accelerated by compressed sensing (CS) are feasible in clinical routine and yield equivalent cardiac morphology in less time. **Design.** We evaluated 155 consecutive patients with various cardiac diseases scanned during our clinical routine. LV and RV short axis (SAX) cine images were acquired by conventional and prototype 2-shot CS sequences on a 1.5T CMR. The 2-shot prototype captures the entire heart over a period of 3 beats making the acquisition potentially even faster. Both scans were performed with identical slice parameters and positions. We compared LV and RV morphology with Bland-Altman plots and weighted the results in relation to pre-defined tolerance intervals. Subjective and objective image quality was evaluated using a 4-point score and adapted standardized criteria. Scan times were evaluated for each sequence. **Results.** In total, no acquisitions were lost due to non-diagnostic image quality in the subjective image score. Objective image quality analysis showed no statistically significant differences. The scan time of the CS cines was significantly shorter ($p < .001$) with mean scan times of 178 ± 36 s compared to 313 ± 65 s for the conventional cine. All cardiac function parameters showed excellent correlation (r 0.978–0.996). Both sequences were considered equivalent for the assessment of LV and RV morphology. **Conclusions.** The 2-shot CS SAX cines can be used in clinical routine to acquire cardiac morphology in less time compared to the conventional method, with no total loss of acquisitions due to nondiagnostic quality.

Trial registration: ISRCTN12344380. Registered 20 November 2020, retrospectively registered.

ARTICLE HISTORY

Received 19 July 2021
Revised 11 June 2022
Accepted 3 July 2022

KEYWORDS

Magnetic resonance imaging; cardiovascular magnetic resonance; compressed sensing; left ventricle; right ventricle; fast imaging

1. Introduction

Cardiovascular magnetic resonance (CMR) has been established as the gold standard for the quantification of the left and right ventricular morphology [1–4]. Quantification of left and right cardiac chambers *via* short-axis (SAX) acquisitions has been shown to be both reliable and accurate [5]. One major drawback is the time-consuming multiple breath-holds needed to acquire a SAX stack using conventional balanced steady-state free precession (bSSFP) sequences [6]. This not only prolongs and impairs the workflow but also puts an increased burden on patients. That becomes even more important as the patient groups having an indication for CMR have an increased likelihood to suffer from cardiac and respiratory insufficiency. Reduced breath-hold capacity can impair the SAX acquisition due to respiratory

or motion artifacts [7–9]. Currently, there are various approaches to increase image acquisition efficiencies. Real-time, single breath-hold or free-breathing sequences and multi-slice acquisition are examples focused on patients with arrhythmias or decreased breath-hold capacities [10–13]. Another approach is based on cine acquisitions accelerated by compressed sensing (CS). CS techniques use incoherent sub-sampling, transform sparsity and iterative reconstruction [14]. They can be either applied to increase spatial resolution or to shorten the acquisition time. We focused on reducing acquisition time by evaluating a prototype 2-shot 2D CS sequence. The 2-shot technique reduces the acceleration factor to 5.6 by capturing 2 heart cycles for the acquisition. A third heart cycle is needed for the preparation. The aim of this study was to evaluate whether quantification of LV and RV function parameters and mass using

CONTACT Jeanette Schulz-Menger  jeanette.schulz-menger@charite.de  DZHK (German Centre for Cardiovascular Research), Partner Site Berlin, Berlin, Germany

 Supplemental data for this article can be accessed online at <https://doi.org/10.1080/14017431.2022.2099010>.

© 2022 The Author(s). Published by Informa UK Limited, trading as Taylor & Francis Group.
This is an Open Access article distributed under the terms of the Creative Commons Attribution-NonCommercial License (<http://creativecommons.org/licenses/by-nc/4.0/>), which permits unrestricted non-commercial use, distribution, and reproduction in any medium, provided the original work is properly cited.

CS in clinical routine yields equivalent results compared to the reference standard. For this purpose, we applied pre-defined tolerance intervals for the LV Quantification by Zange et al. [15] and, for the first time, established such tolerance intervals for RV Quantification.

2. Material and methods

2.1. Study population

In this study, we included 155 consecutive patients from our clinical routine with an indication for CMR and no general contraindications [16]. All patients were in sinus rhythm during the exam. The patients had the following indications for CMR: coronary artery disease ($N=101$; 65%), myocarditis ($N=39$; 25%), structural heart disease ($N=13$; 8%), valvular heart disease ($N=1$; 1%), cardiac tumor ($N=1$; 1%). Wall-motion abnormalities were assessed for each patient in both sequences according to current guidelines [17]. We compared the conventional and the CS sequences in terms of: 1) clinical left and right ventricular function parameters and mass, 2) subjective and objective image quality (SIQ and OIQ, respectively) criteria and 3) scan time. Ethical approval was obtained from the local ethics committee of Charité Medical University Berlin (approval number EA1/367/20).

2.2. Imaging protocol

All scans were acquired on a 1.5 Tesla scanner (MAGNETOM Avanto^{-FIT}, Siemens Healthineers, Erlangen, Germany). All patients underwent a state-of-the-art segmented 2D bSSFP cine sequence accelerated by an acceleration factor of 2 with multiple breath-holds which served as the reference method. In addition, a prototype 2-shot segmented 2D bSSFP CS cine sequence was used to acquire a second SAX stack [18]. The reconstruction framework of the CS cine sequence was based on a previously published article [19]. All reconstruction work was in-line, with the images being directly sent to the workstation for post-processing. The acceleration factor for the CS cine sequence was chosen to result in the best compromise between scan time and image quality. The conventional cine sequence was performed first, followed directly by the CS cine sequence. 128 (82.6%) of the acquisitions were performed after contrast agent application and 27 (17.4%) before. For both sequences, slice planning and position as well as gap and thickness were identical and according to institutional standards. One slice was acquired per breath-hold. The number of slices was adjusted for ventricular size and clinical indication, ranging from 12 to 22. Imaging parameters are listed in Table 1.

2.3. Assessment of cardiac morphology

Both acquisitions were analysed using dedicated software (circle CVI⁴² version 5.6.2, Calgary, Canada). Manual contouring in SAX cine images was used to assess left

Table 1. Imaging parameters of the reference bSSFP cine sequence and the CS cine sequence.

Parameter	Conventional bSSFP cine	CS bSSFP 2-shot cine
TR (ms)	3.31	2.81
TE (ms)	1.44	1.19
Flip angle (°)	80	55
Spatial resolution (mm ²)	2.0 × 2.0	1.6 × 1.6
Temporal resolution (ms)	46.34	44.96
FOV (mm ²)	380.00 × 308.75	380.00 × 304.00
Matrix (pixels ²)	192 × 156	240 × 192
Bandwidth (Hz/pixel)	930	930
Slice thickness/gap (mm)	7/0	7/0
Cardiac phases (n)	30	25
Breath-hold	11 heart beats/slice	3 heart beats/slice*
ECG gating	retrograde	retrograde

bSSFP: balanced steady state free precession; CS: compressed sensing; TR: time of repetition; TE: echo time; FOV: field of view; ECG: electrocardiogram. *1 heartbeat is used for the preparation and 2 (therefore called 2-shot) for the acquisition.

ventricular ejection fraction (LVEF), stroke volume (LVSV), end-diastolic volume (LVEDV), end-systolic volume (LVESV), ventricular mass (LVM) as well as right ventricular ejection fraction (RVEF), stroke volume (RVSV), end-diastolic volume (RVEDV) and end-systolic volume (RVESV). All contours were drawn in accordance with the latest consensus statement for postprocessing [17]. In the LV, papillary muscles were manually contoured in end-diastolic and end-systolic phases and were included in the myocardium. LVM was assessed in end-diastole (LVMd) and end-systole (LVMs) using epicardial contours. RV end-diastolic and end-systolic contours were drawn in the corresponding LV phases. The basal slice of the RV was determined by checking for the presence of the pulmonary valve or the enlargement of the right ventricular cavity during diastole to avoid contouring the right atrium (RA) [20]. RV trabeculae and papillary muscles were included in the RV blood pool volume in diastole and systole. To assess whether contrast-media application influenced function and volume assessment, the absolute differences between conventional cines and CS cines for pre-and post-contrast media scans were compared.

2.4. Image quality assessment

Image quality was assessed visually. For SIQ analysis an established 4-point scale was used (4= excellent, no artifacts; 3= good, minor artifacts; 2= moderate, some artifacts; 1= poor, nondiagnostic due to artifacts), as described previously [21]. For the OIQ assessment, a standardized item catalogue as described by Klinke et al. was used [22] and our adapted approach is outlined here shortly: image quality was rated based on an 8 quality criteria including LV coverage (max. 5 points), wrap-around, respiratory ghost, cardiac ghost, metal artifacts, shimming artifacts (total sum max. 3 points), signal loss and orientation of stack (each max. 2 points). The subpoint “image blurring/mis-triggering” [22] was excluded. Items 10–12 of the standardized image criteria were not assessed as they have been the same for both acquisitions and so an overall maximum score of 12 could

be achieved [22]. A higher score indicated worse image quality.

2.5. Scan time assessment

Scan time was assessed by calculating total scan time defined as the sequence time duration from the first to the last slice. For both sequences, breath-holds and breath-hold commands were included, with a single slice-single breath hold approach.

2.6. Statistical analysis

All continuous variables (LVEF, LVSV, LVEDV, LVESV, LVMD, LVMS, RVEF, RVS, RVEDV, RVESV and scan time) and their differences are represented as mean and \pm standard deviation (SD) with 95%-confidence intervals. Normal distribution was visually assessed by means of histograms and QQ-plots. No major deviations from normal distribution were detected so the paired Students *t*-test was used to test for statistical significance. A *p* value $< .05$ was considered to indicate a statistically significant difference for the assessed parameters. The Pearson's correlation coefficient (*r*) was used to assess the correlation between the values obtained from both sequences for each individual parameter. Bland-Altman plots were generated to assess the mean difference and the 95%-limits of agreement between the two sequences. Equivalence testing, as previously described by Zange et al. [15], was carried out for all quantified LV parameters using the published 95%-tolerance intervals. In a similar approach, we established such limits of equivalence for the RV as follows: RV quantification, using SAX cine sequences from a heterogeneous patient group consisting of 77 patients was carried out twice by the same reader with an interval of more than two months. Mean and standard deviations were computed for the intra-observer deviations of each quantified parameter (RVEF, RVS, RVEDV and RVESV). Given a sufficiently normal distribution of these differences, RV tolerance intervals have been calculated as ± 1.96 times the standard deviation. The reference and CS sequences were considered equivalent for an examined parameter if the 95%-confidence interval of its difference was entirely within the limits of the 95%-tolerance intervals. SIQ and OIQ are given as classes. Image quality variables were tested using the Wilcoxon signed-rank test. Statistical analysis was performed using dedicated software (SPSS version 26, International Business Machines, Armonk, New York, USA). Bland-Altman plots and tolerance intervals were constructed using Graph Pad Prism 9, version 9.0.0 (GraphPad Software, La Jolla, California, USA).

3. Results

3.1. Study population

155 bSSFP and CS SAX acquisitions were analysed. After an interim analysis of 111 patients (111/155, 71.6%), 44 additional patients with an LVEF $< 30\%$ were scanned

Table 2. Patient characteristics and comorbidities.

	Mean \pm SD
Age (years)	59.9 \pm 14.9
Sex (male/female)	94/61 (61% / 39%)
Height (cm)	172.9 \pm 9.4
Weight (kg)	80.4 \pm 16.8
BMI (kg/m ²)	26.8 \pm 4.8
BSA (m ²)	1.9 \pm 0.2
EF (%)	N (%)
>50	91 (59%)
40–50	24 (15%)
30–40	20 (13%)
<30	20 (13%)
Comorbidities	N (%)
Arterial hypertension (HTN)	75 (48.4%)
Coronary artery disease (CAD)	62 (40%)
Congestive heart failure (CHF)	54 (34.8%)
Diabetes Mellitus (DM)	27 (1.4%)
Valvular heart disease (VHD)	31 (20%)
Chronic kidney disease (CKD)	20 (12.9%)
Hyperlipidaemia (HLD)	53 (34.2%)
Peripheral artery disease (PAD)	12 (7.7%)
Cardiomyopathy (CM)	16 (10.3%)
Lung disease (LD)	25 (16.1%)

SD: standard deviation; BMI: body mass index; BSA: body surface area; EF: Ejection Fraction.

prospectively to ensure coverage of the entire range of LV function. Patient characteristics and comorbidities are given in Table 2. Regional wall motion abnormalities were observed in 15%.

3.2. Left and right ventricular function parameters and mass

Comparing the cardiac function parameters and mass of the CS SAX acquisition with the conventional method by applying modified Bland-Altman plots, we found a good correlation as well as no systematic biases between the two (Figure 1 for left ventricular and Figure 2 for right ventricular function and mass parameters). Both sequences can be considered equivalent for the quantification of biventricular function in the SAX (Table 3) (Figure 3). Our definition of tolerance intervals for the RV is outlined in the methodology part with the corresponding margins given in Table 4. The equivalence testing was performed as described by Zange et al. [15]. The 95%-confidence intervals for all LV and RV function parameters and mass (black lines in Figure 3) were completely contained within their corresponding 95%-tolerance intervals (grey shaded areas in Figure 3) showing no clinically relevant differences. Larger volumes were observed using the conventional cine sequence for all functional variables while myocardial mass was overestimated in diastole by 5.42 ± 8.41 (g) and systole by 0.82 ± 6.45 (g) applying the prototype CS cine sequence. Comparing the differences in function and mass assessment between pre- and post-contrast media acquisitions for conventional and CS cines the following results can be reported: (mean \pm SD [95% CI]) for differences in: LVEF: pre-contrast $0.54\% \pm 2.54$ [−0.47 to 1.55]; post-contrast $0.25\% \pm 2.19$ [−0.13 to 0.64] *p* = .590; LVSV: pre-contrast $0.97 \text{ ml} \pm 4.93$ [−0.98 to 2.92]; post-contrast $1.62 \text{ ml} \pm$

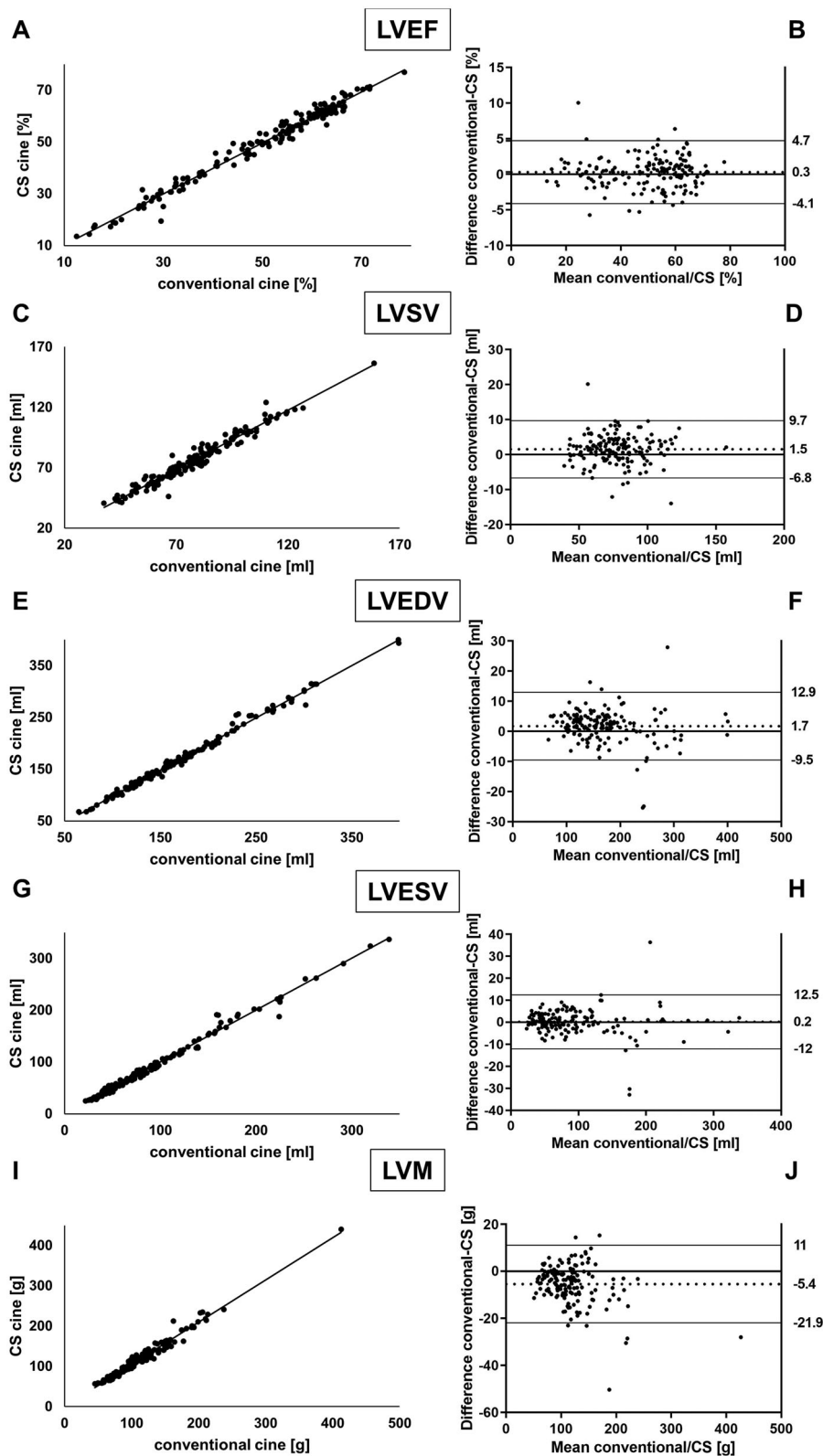


Figure 1. Scatter plots and modified Bland-Altman plots for left ventricular function. Scatter plots displaying a good correlation for left ventricular function and volume parameters for the conventional and the CS (compressed sensing) cine (LVEF (1A), LVSV (1C), LVEDV (1E), LVESV (1G), LVM (1I)). Modified Bland-Altman plots of difference between LV functional parameters for agreement between conventional and CS cine images for LVEF (1B), LVSV (1D), LVEDV (1F), LVESV (1H), LVM (1J). Dashed lines indicate mean difference, dotted lines indicate 95%-limits of agreement.

4.02 [0.92 to 2.32] $p = .52$; LVEDV: pre-contrast $-1.1 \text{ ml} \pm 6.77$ [-3.77 to 1.59]; post-contrast $2.32 \text{ ml} \pm 5.33$ [1.4 to 3.26] $p = .019$; LVESV: pre-contrast $-2.1 \text{ ml} \pm 9.2$ [-5.7 to 1.58]; post-contrast $0.71 \text{ ml} \pm 5.36$ [-0.23 to 1.64] $p = .141$;

LVMD: pre-contrast $-6.15 \text{ g} \pm 7.95$ [-9.3 to 3.01]; post-contrast $-5.27 \text{ g} \pm 8.54$ [-6.76 to -3.77] $p = .606$; RVEF: pre-contrast $0.8\% \pm 1.93$ [-0.69 to 0.84]; post-contrast $-0.01\% \pm 2.04$ [-0.36 to 0.35] $p = .846$; RVSF: pre-

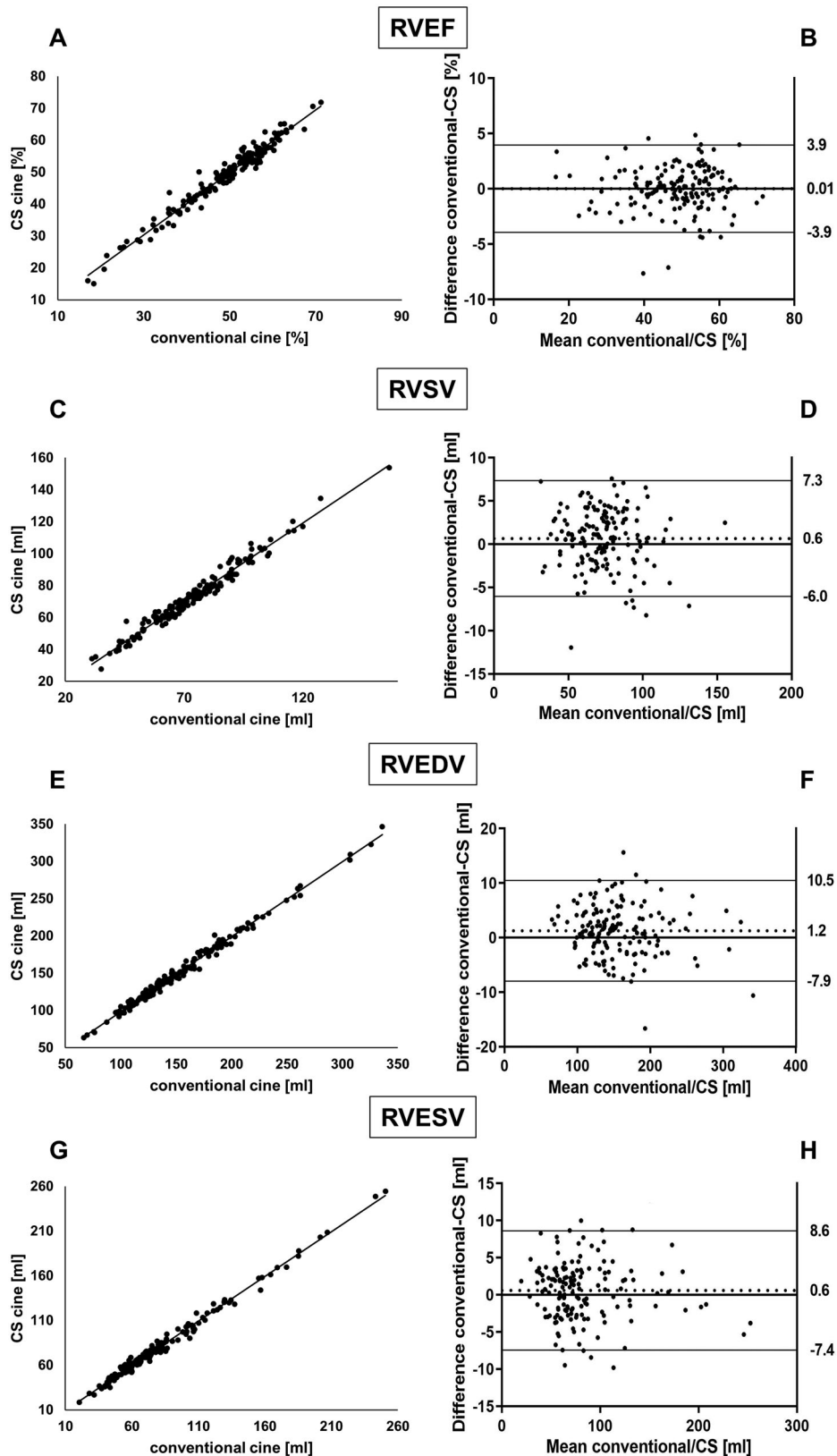


Figure 2. Scatter plots and modified Bland-Altman plots for right ventricular function. Scatter plots displaying a good correlation for right ventricular function and volume parameters for the conventional and the CS (compressed sensing) cine (RVEF (2A), RVSV (2C), RVEDV (2E), RVESV (2G)). Modified Bland-Altman plots of difference between RV functional parameters for agreement between conventional and CS cine images for RVEF (2B), RVSV (2D), RVEDV (2F), RVESV (2H). Dashed lines indicate mean difference, dotted lines indicate 95%-limits of agreement.

contrast $0.59 \text{ ml} \pm 3.79$ $[-0.91 \text{ to } 2.1]$; post-contrast $0.68 \text{ ml} \pm 3.36$ $[0.09 \text{ to } 1.27]$ $p = .907$; RVEDV: pre-contrast 3.8 $[-1.5 \text{ to } 1.48]$; post-contrast $0.72 \text{ ml} \pm 4.15$ $[-0.01 \text{ to } 1.44]$ $p = .368$.

Table 3. Left and right ventricular function parameters and mass.

Parameter	conventional cine (mean ± SD; [95% CI])	CS cine (mean ± SD; [95% CI])	Differences (mean ± SD; [95% CI])	95%-Tolerance intervals (±)*	Confidence interval of the difference contained within the 95%-tolerance intervals (yes/no)	Pearson's correlation coefficient (r)	p
LVEF (%)	50.01 ± 14.69 [47.68 to 52.34]	49.71 ± 14.64 [47.38 to 52.03]	0.30 ± 2.25; [-0.05 to 0.66]	5.3	Yes	0.988	.096
LVSF (ml)	78.39 ± 19.99 [75.22 to 81.57]	76.89 ± 19.98 [73.71 to 80.06]	1.50 ± 4.18; [0.84 to 2.17]	4.5	Yes	0.978	<.001
LVEDV (ml)	171.05 ± 64.53 [160.81 to 181.29]	169.32 ± 65.41 [158.94 to 179.70]	1.73 ± 5.73; [0.82 to 2.64]	10.8	Yes	0.996	<.001
LVESV (ml)	92.65 ± 62.06 [82.8 to 102.5]	92.43 ± 62.56 [82.50 to 102.35]	0.22 ± 6.24; [-0.76 to 1.21]	7.3	Yes	0.995	.654
LVMd (g)	114.98 ± 44.09 [107.98 to 121.97]	120.4 ± 46.9 [112.96 to 127.84]	-5.42 ± 8.41; [-6.75 to -4.08]	13.3	Yes	0.985	<.001
LVMs (g)	121.99 ± 48.37 [114.18 to 129.79]	122.81 ± 47.68 [115.11 to 130.5]	-0.82 ± 6.45 [-1.86 to 0.22]	13.3	Yes	0.991	.119
RVEF (%)	48.74 ± 10.36 [47.09 to 50.38]	48.73 ± 10.33 [47.09 to 50.37]	0.01 ± 2.01; [-0.31 to 0.32]	5.3	Yes	0.981	.956
RVSF (ml)	73.47 ± 19.7 [70.34 to 76.59]	72.8 ± 19.94 [69.84 to 75.97]	0.66 ± 3.14; [0.12 to 1.2]	13.22	Yes	0.985	.017
RVEDV (ml)	156.01 ± 47.9 [148.41 to 163.61]	154.76 ± 48.49 [147.07 to 162.45]	1.25 ± 4.71; [0.5 to 1.99]	14.56	Yes	0.995	.001
RVESV (ml)	82.54 ± 39.71 [76.24 to 88.84]	81.95 ± 39.84 [75.63 to 88.27]	0.58 ± 4.09; [-0.06 to 1.23]	9.69	Yes	0.995	.075

bSSFP: balanced steady-state free precession; CS: compressed sensing; LVEF: left ventricular ejection fraction; LVSF: left ventricular stroke volume; LVEDV: left ventricular end-diastolic volume; LVESV: left ventricular end-systolic volume; LVMd: diastolic left ventricular myocardial mass; LVMs: systolic left ventricular myocardial mass; RVEF: right ventricular ejection fraction; RVSF: right ventricular stroke volume; RVEDV: right ventricular end-diastolic volume; RVESV: right ventricular end-systolic volume. *Tolerance intervals for the LV based on Zange et al. [15], for the RV based on 1.96*SD.

3.3. Image quality

Comparing the conventional and the CS cines using the adapted standardized OIQ criteria [22], no statistically significant differences were detected (median 0 and 0 respectively, $p = .174$) (Supplementary Table 1). The majority of the conventional acquisitions were rated with zero total points (140/155; 90.3%) compared to 136/155 (87.7%) for the CS cines. 9 scans with the conventional cine were rated with one point (9/155; 5.8%) and 6 with two points (6/155; 3.9%). No scan with the conventional cine was rated with more than two points. The images acquired with the CS sequence showed a more heterogenic distribution with 10 scans being rated with one point (10/155; 6.5%), one scan with two points (1/155; 0.6%), 7 with three points (7/155; 4.5%) and one with four points (1/155; 0.6%). Neither a conventional nor a CS cine scored more than four points in total. Supplementary Table 2 summarizes the findings for non-zero scores. There was neither a difference in OIQ for the conventional cines regarding pre- and post-contrast media acquisitions ($p = .396$) nor for the CS acquisitions pre- and post-contrast ($p = .844$).

SIQ analysis revealed a statistically significant difference between conventional and CS cine images (median 4 and 3 respectively, $p < .001$) (Supplementary Table 3). The majority of the conventional cine acquisitions were rated excellent (116/155; 74.8%). The most common rating for CS acquisitions was excellent (65/155; 41.9%). CS cine scans were rated moderate 32 times (20.6%) compared to nine acquisitions by the conventional approach rated moderate (5.8%). Only two acquisitions were rated nondiagnostic, these were different ones for the conventional and CS sequences (Supplementary Figure 1). On average, there was no total loss in image acquisitions. Examples are given for excellent, good and moderate image quality (Figure 4). Examples with an increased blurry aspect are shown in supplementary Figure 2. SIQ did not differ for conventional cines ($p = .846$) or CS cines ($p = .203$) pre- and post-contrast media application.

3.5 Scan time.

Mean cine scan times (± SD) [95% CI] for the conventional and CS sequences were 313 (± 65 s) [303–324] (range 172–542) and 178 (± 36 s) [172–184] (range 106–304) respectively ($p < .0001$) (Figure 5). This results in an average scan time of $19 ± 3$ s per slice for conventional images in comparison to $11 ± 2$ s per slice for CS images.

4. Discussion

Our main results are: Firstly, the conventional sequence and the new 2-shot CS sequence are equivalent for LV and RV function and LV mass assessment. Secondly, all image acquisitions, except one, obtained by the conventional sequence and the CS sequence had diagnostic image quality leading to no total loss due to nondiagnostic quality.

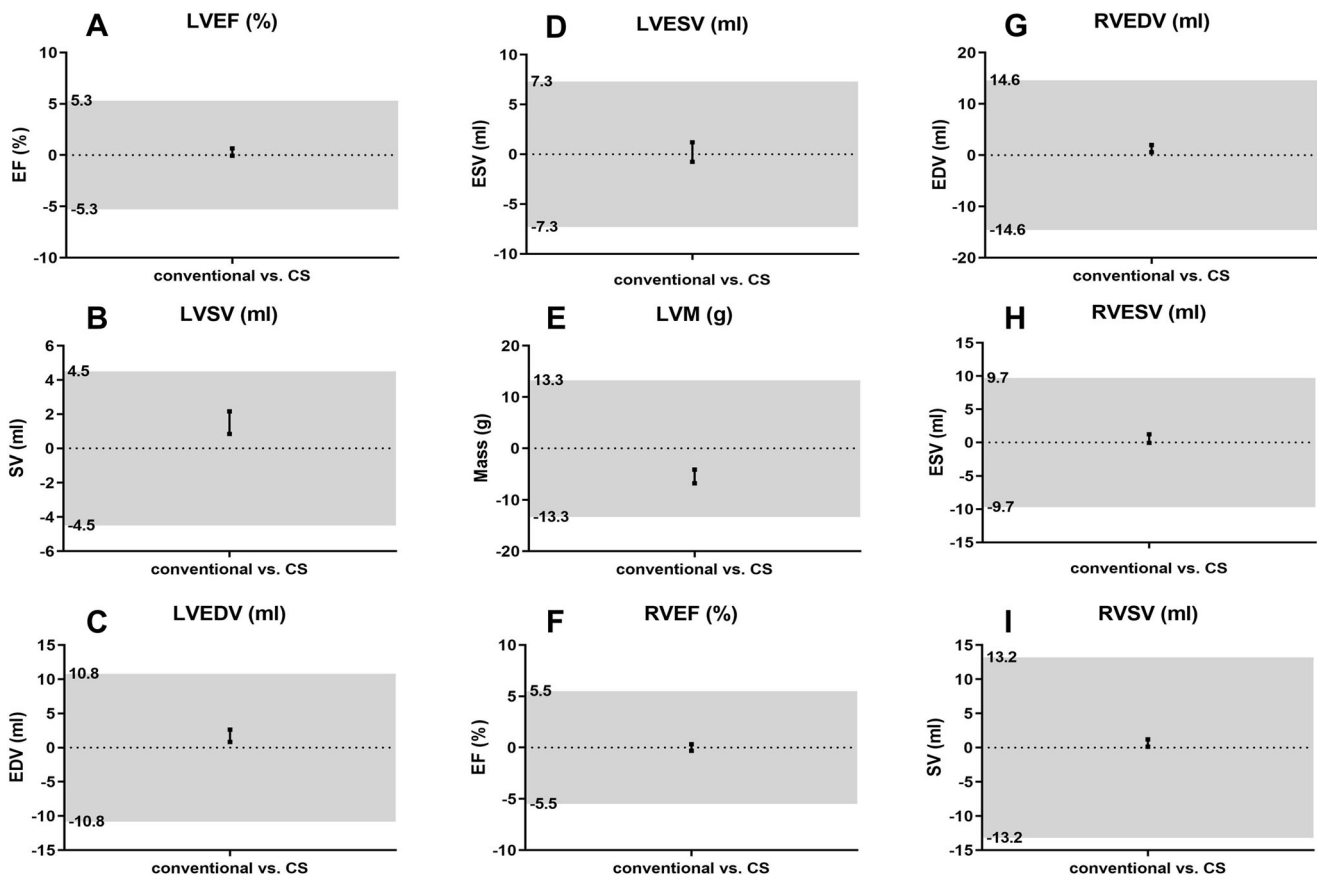


Figure 3. Equivalence testing for the left and right ventricle. Equivalence testing for LVEF (3A), LVSV (3B), LVEDV (3C), LVESV (3D), LVM (3E), RVEF (3F), RVSV (3G), RVEDV (3H), RVESV (3I). Equivalence of measurements between the two sequences is shown if the 95%-confidence interval for the difference between sequences (indicated as black lines, squares marked upper and lower limits) are contained within the 95%-tolerance limits (tolerance intervals marked grey).

Table 4. Right ventricular tolerance intervals.

Parameter	Tolerance intervals (\pm)*
RVEF (%)	5.53
RVSV (ml)	13.22
RVEDV (ml)	14.56
RVESV (ml)	9.69

RVEF: right ventricular ejection fraction; RVSV: right ventricular stroke volume; RVEDV: right ventricular end-diastolic volume; RVESV: right ventricular end-systolic volume, *calculated as $1.96 \times$ standard deviation.

Finally, using the prototype CS sequence in clinical routine is significantly faster than the reference sequence.

In the past most publications concerning approaches to increase scan efficiency have focused on Real Time (RT) sequences or acquisitions accelerated by CS with single breath holds or free breathing [10,11,23–27]. Recently there has been an increase in published literature covering the implication of 2D segmented CS cine sequences with retro-gate gating for the analysis of biventricular function (e.g. LVEF, RVEF) and volumetric parameters (e.g. EDV, ESV, SV and cardiac output) [28,29]. In addition to these standardized parameters, there has been also research carried out regarding atrial functional parameters (e.g. left and right atrial size and emptying fractions) [30]. The overall results show a good correlation between conventional and CS cines with the advantage of a significant time reduction. We could confirm these findings in a larger patient cohort. As the

acquisitions were embedded in the clinical routine our population covers the entire clinical EF range (12–78%) as well as a variety of cardiac diseases. Independent of the underlying pathology or the level of functional impairment (based on the LVEF) both sequences showed a good correlation between cardiac function and mass assessment (Figures 1 and 2). Equivalence testing showed the complete equivalence of all parameters quantified using the conventional method and the CS cine (Figure 3). Accordingly, we attribute the measured differences to the intraobserver variability. We, therefore, conclude that the differences in measurements in the two sequences are not relevant to clinical routine. The larger values for LVM using CS are most likely due to the difficulty of identifying the epicardial border being caused by the blurring of the images. Proper mass assessment is especially important for the differential diagnosis of left ventricular hypertrophies, which are a common indication for CMR referral. To resolve this issue the additional time gained by the 2-shot CS sequence in comparison to the conventional cine could be spent on acquiring a higher spatial resolution potentially improving the blurry aspect with sharper myocardial edges.

In total, there was no loss of acquisitions as both sequences had one scan rated as nondiagnostic. The lower SIQ scores could be attributed to the relatively blurry appearance of the CS images. Image sharpness was measured in previous studies [18,29]. Overall, the findings suggest a clear

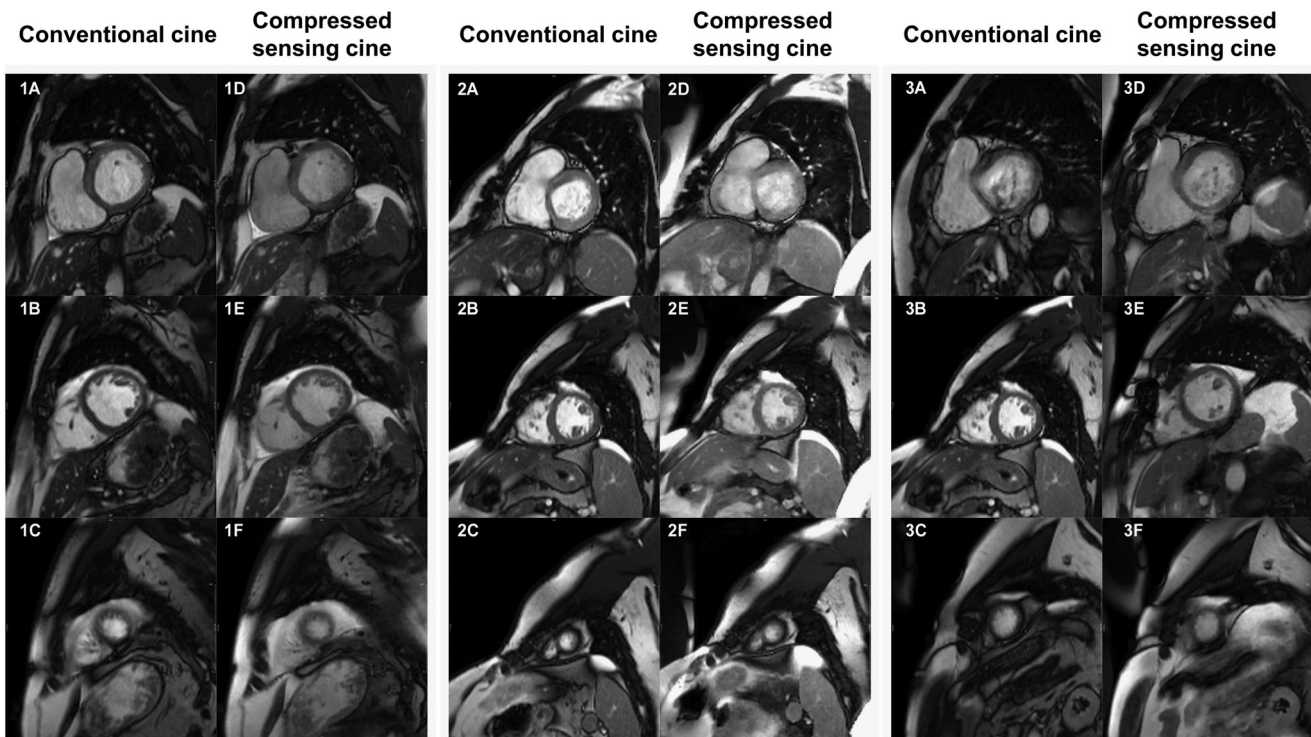


Figure 4. Examples of conventional and CS cine acquisitions are rated as excellent (=4), good (=3) and moderate (=2). Examples of conventional and CS cine acquisitions rated as excellent (=4) ((1A–1C), (1D–1F), respectively), as good (=3) (2A–2C), (2D–2F) and as moderate (=2) (3A–3C), (3D–3F). Shown are basal, mid-ventricular and apical slices, respectively. Basal slices in both acquisitions rated as moderate (3A,3D) had artefacts impairing the detection of the left-ventricular outflow tract.

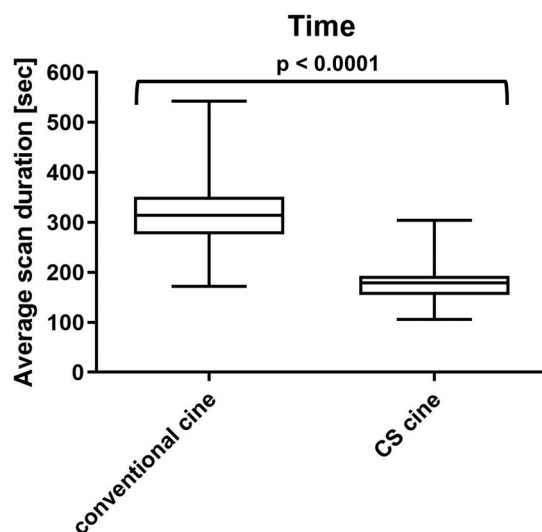


Figure 5. Boxplots comparing average time per scan for conventional and CS cine images. Boxplots showing the average scan duration in seconds for conventional and CS cine images, respectively. Whiskers indicate the minimum and maximum values. Lines represent the 25th percentile, median and 75th percentile in ascending order.

improvement in image sharpness between RT and segmented 2D CS cines with retrograde gating [24] whereas a small to no improvement between conventional and CS cines [29,30]. By adapting the objective image criteria, we could show that the CS image quality in fact is not worse than the conventional approach. Even despite the lower SIQ, we were able to adequately quantify the RV with very small differences in the absolute values. Therefore, we are

positive about future directions regarding artificial intelligence and the ability for a detailed and precise assessment of RV ventricular appendages and trabeculae. As a non-ionizing method with good interstudy reliability for the RV assessment [31] and comparable tolerance intervals for the left and right ventricles, as shown in this study, CS sequences could be a fast tool for regular follow-up examinations in a diverse group of patients. Further studies with a focus on certain subgroups are needed to establish this approach for the specific indications. In the light of rapid advances in CMR with new sequences and techniques such as mapping, exam time increases, thereby reducing the patient's comfort and cooperation [32,33]. To shorten the exam time we routinely perform the acquisition of SAX directly after the application of contrast agents to effectively use the time before late gadolinium enhancement (LGE) images. This procedure [34] is increasingly used and has been recommended in the setup of rapid protocols [16]. The results of the comparison between pre- and post-contrast media application show that this has no effect on the image quality and does not impair reliable function and mass assessment despite a lower myocardium-to-blood-contrast. The statistically significant differences regarding the LVEDV could most likely be attributed to the increased difficulty of a proper delineation of papillary muscles and trabecular appendages in the left ventricle after contrast media application due to the increased intensity/brightness. However, no such differences were observed in regard to LVESV or RV assessment and the absolute differences were small and well within the tolerance margins.

We demonstrated that the time needed for cine acquisitions with 2-shot CS cine is significantly shorter and was reduced by approximately 50% in comparison to the conventional cine sequence. There is a possibility to decrease scan time even further by either scanning more than one slice in a single-breath hold or applying a single-shot technique to CS sequences [18]. This however leads to a trade-off between image quality and acquisition time. Current work suggests that the CS single-shot technique is marginally faster than the 2-shot sequence but provides a lower image quality than conventional cines [18] and lower edge sharpness [35]. Picking up on the aspect of reduced breath hold capacity mentioned in the introduction we want to underline that any decrease in scan time has a beneficial value for the patients undergoing CMR exams. This benefit is especially evident in larger and longer ventricles where more slices are needed to cover the entire heart. Reducing breath holds therefore might be another approach to decrease scan time. Kido et al. demonstrated this by capturing 8 slices in one breath hold [11]. The results are very promising however we want to point out that 8 slices might not be enough to capture the entire ventricle in patients with dilated heart chambers if scanned with zero gap.

4.1. Limitations

The main limitation of this study is that it was conducted as a single-center study. Another limitation is that the tolerance intervals for the RV were defined by a single observer. Additionally, attention should be drawn to the fact that the standardized objective criteria have been only assessed for the LV without taking the RV into consideration.

5. Conclusion

Using CS sequences to acquire SAX cine stacks can improve the workflow by shortening the individual scan time per patient. The use of the CS technique should be considered particularly in routine cases when a detailed assessment of ventricular structure is not required as well as in patients who have difficulty holding their breath for longer periods of time. Further studies with larger patient cohorts are needed to validate the CS-derived parameters in clinical routine and to assess how precisely CS sequences detect more subtle aetiologies. This is especially of importance regarding left ventricular hypertrophies as we noticed an overestimation of the LVM by the CS sequence.

Acknowledgements

We gratefully thank our CMR technicians Kerstin Kretschel, Denise Kleindienst and Martina Kohla for technical assistance as well as our study nurses Annette Köhler and Elke Nickel-Szczzech. The whole Working Group CMR was involved and we are thankful for the input on different levels. We thank Carsten Schwenke Ph.D. for his support in matters of study statistics.

Disclosure statements

The authors report no declarations of interest.

Funding

The work of Jan Gröschel has received funding from the EMPIR program co-financed by the Participating States and from the European Union's Horizon 2020 research and innovation program (18HLT05 QUIERO, 2020). Prof. Schulz-Menger holds institutional grants from the Charité Medical University.

ORCID

Jan Gröschel  <http://orcid.org/0000-0002-7268-9041>

Clemens Ammann  <http://orcid.org/0000-0002-5962-4008>

References

- [1] Kawel-Boehm N, Maceira A, Valsangiacomo-Buechel ER, et al. Normal values for cardiovascular magnetic resonance in adults and children. *J Cardiovasc Magn Reson*. 2015;17:29.
- [2] Petersen SE, Aung N, Sanghvi MM, et al. Reference ranges for cardiac structure and function using cardiovascular magnetic resonance (CMR) in Caucasians from the UK biobank population cohort. *J Cardiovasc Magn Reson*. 2017;19(1):18.
- [3] Couto M, Souto M, Martinez A, et al. Accuracy of right ventricular volume and function assessed with cardiovascular magnetic resonance: comparison with echocardiographic parameters. *Clin Imaging*. 2020;59(1):61–67.
- [4] Gardner BI, Bingham SE, Allen MR, et al. Cardiac magnetic resonance versus transthoracic echocardiography for the assessment of cardiac volumes and regional function after myocardial infarction: an intrasubject comparison using simultaneous intrasubject recordings. *Cardiovasc Ultrasound*. 2009;7(1):38.
- [5] Grothues F, Moon JC, Bellenger NG, et al. Interstudy reproducibility of right ventricular volumes, function, and mass with cardiovascular magnetic resonance. *Am Heart J*. 2004;147(2):218–223.
- [6] Lin ACW, Strugnell W, Riley R, et al. Higher resolution cine imaging with compressed sensing for accelerated clinical left ventricular evaluation. *J Magn Reson Imaging*. 2017;45(6):1693–1699.
- [7] Alfudhili K, Masci PG, Delacoste J, et al. Current artefacts in cardiac and chest magnetic resonance imaging: tips and tricks. *Br J Radiol*. 2016;89(1062):20150987.
- [8] Ferreira PF, Gatehouse PD, Mohiaddin RH, et al. Cardiovascular magnetic resonance artefacts. *J Cardiovasc Magn Reson*. 2013;15:41.
- [9] van der Graaf AW, Bhagirath P, Ghoerbien S, et al. Cardiac magnetic resonance imaging: artefacts for clinicians. *Neth Heart J*. 2014;22(12):542–549.
- [10] Cui C, Yin G, Lu M, et al. Retrospective electrocardiography-gated real-time cardiac cine MRI at 3T: comparison with conventional segmented cine MRI. *Korean J Radiol*. 2019;20(1):114–125.
- [11] Kido T, Kido T, Nakamura M, et al. Compressed sensing real-time cine cardiovascular magnetic resonance: accurate assessment of left ventricular function in a single-breath-hold. *J Cardiovasc Magn Reson*. 2016;18(1):50.
- [12] Stab D, Ritter CO, Breuer FA, et al. CAIPIRINHA accelerated SSFP imaging. *Magn Reson Med*. 2011;65(1):157–164.
- [13] Usman M, Atkinson D, Heathfield E, et al. Whole left ventricular functional assessment from two minutes free breathing multi-slice CINE acquisition. *Phys Med Biol*. 2015;60(7):N93–107.

- [14] Lustig M, Donoho D, Pauly JM. Sparse MRI: the application of compressed sensing for rapid MR imaging. *Magn Reson Med*. 2007;58(6):1182–1195.
- [15] Zange L, Muehlberg F, Blaszczyk E, et al. Quantification in cardiovascular magnetic resonance: agreement of software from three different vendors on assessment of left ventricular function, 2D flow and parametric mapping. *J Cardiovasc Magn Reson*. 2019;21(1):12.
- [16] Kramer CM, Barkhausen J, Bucciarelli-Ducci C, et al. Standardized cardiovascular magnetic resonance imaging (CMR) protocols: 2020 update. *J Cardiovasc Magn Reson*. 2020;22(1):17.
- [17] Schulz-Menger J, Bluemke DA, Bremerich J, et al. Standardized image interpretation and post-processing in cardiovascular magnetic resonance – 2020 update: society for cardiovascular magnetic resonance (SCMR): board of trustees task force on standardized post-processing. *J Cardiovasc Magn Reson*. 2020;22(1):19.
- [18] Wang J, Li X, Lin L, et al. Diagnostic efficacy of 2-shot compressed sensing cine sequence cardiovascular magnetic resonance imaging for left ventricular function. *Cardiovasc Diagn Ther*. 2020;10(3):431–441.
- [19] Liu J, Lefebvre A, Zenge MO, et al. 2D bSSFP real-time cardiac CINE-MRI: compressed sensing featuring weighted redundant haar wavelet regularization in space and time. *J Cardiovasc Magn Reson*. 2013;15(S1):P49–P.
- [20] Hudsmith LE, Petersen SE, Francis JM, et al. Normal human left and right ventricular and left atrial dimensions using steady state free precession magnetic resonance imaging. *J Cardiovasc Magn Reson*. 2005;7(5):775–782.
- [21] Morita K, Utsunomiya D, Oda S, et al. Comparison of 3D phase-sensitive inversion-recovery and 2D inversion-recovery MRI at 3.0 T for the assessment of late gadolinium enhancement in patients with hypertrophic cardiomyopathy. *Acad Radiol*. 2013;20(6):752–757.
- [22] Klinker V, Muzzarelli S, Lauriers N, et al. Quality assessment of cardiovascular magnetic resonance in the setting of the European CMR registry: description and validation of standardized criteria. *J Cardiovasc Magn Reson*. 2013;15(1):55.
- [23] Kido T, Kido T, Nakamura M, et al. Assessment of left ventricular function and mass on free-breathing compressed sensing real-time cine imaging. *Circ J*. 2017;81(10):1463–1468.
- [24] Vermersch M, Longere B, Coisne A, et al. Compressed sensing real-time cine imaging for assessment of ventricular function, volumes and mass in clinical practice. *Eur Radiol*. 2020;30(1):609–619.
- [25] Vincenti G, Monney P, Chaptinel J, et al. Compressed sensing single-breath-hold CMR for fast quantification of LV function, volumes, and mass. *JACC Cardiovasc Imaging*. 2014;7(9):882–892.
- [26] Hong S, Hong K, Culver AE, et al. Highly accelerated real-time free-breathing cine CMR for patients with a cardiac implantable electronic device. *Acad Radiol*. 2021;28(12):1779–1786.
- [27] Allen BD, Carr ML, Markl M, et al. Accelerated real-time cardiac MRI using iterative sparse SENSE reconstruction: comparing performance in patients with sinus rhythm and atrial fibrillation. *Eur Radiol*. 2018;28(7):3088–3096.
- [28] Naresh NK, Malone L, Fujiwara T, et al. Use of compressed sensing to reduce scan time and breath-holding for cardiac cine balanced steady-state free precession magnetic resonance imaging in children and young adults. *Pediatr Radiol*. 2021;51(7):1192–1201.
- [29] Longere B, Gkizas CV, Coisne A, et al. 60-S retrogated compressed sensing 2D cine of the heart: sharper borders and accurate quantification. *J Clin Med*. 2021;10(11):2417.
- [30] Altmann S, Halfmann MC, Abidoye I, et al. Compressed sensing acceleration of cardiac cine imaging allows reliable and reproducible assessment of volumetric and functional parameters of the left and right atrium. *Eur Radiol*. 2021;31(10):7219–7230.
- [31] Blalock SE, Banka P, Geva T, et al. Interstudy variability in cardiac magnetic resonance imaging measurements of ventricular volume, mass, and ejection fraction in repaired tetralogy of fallot: a prospective observational study. *J Magn Reson Imaging*. 2013;38(4):829–835.
- [32] Messroghli DR, Moon JC, Ferreira VM, et al. Clinical recommendations for cardiovascular magnetic resonance mapping of T1, T2, T2* and extracellular volume: a consensus statement by the society for cardiovascular magnetic resonance (SCMR) endorsed by the European Association for Cardiovascular Imaging (EACVI). *J Cardiovasc Magn Reson*. 2018;20(1):9.
- [33] Saeed M, Van TA, Krug R, et al. Cardiac MR imaging: current status and future direction. *Cardiovasc Diagn Ther*. 2015;5(4):290–310.
- [34] Sorensson P, Heiberg E, Saleh N, et al. Assessment of myocardium at risk with contrast enhanced steady-state free precession cine cardiovascular magnetic resonance compared to single-photon emission computed tomography. *J Cardiovasc Magn Reson*. 2010;12(1):25.
- [35] Zou Q, Xu HY, Fu C, et al. Utility of single-shot compressed sensing cardiac magnetic resonance cine imaging for assessment of biventricular function in free-breathing and arrhythmic pediatric patients. *Int J Cardiol*. 2021;338:258–264.